IEEE Access
Multidisciplinary : Rapid Review : Open Access Journal

Received May 13, 2020, accepted June 13, 2020, date of publication June 19, 2020, date of current version July 2, 2020.

Digital Object Identifier 10.1109/ACCESS.2020.3003676

On-Chip Electro-Optic Modulator With Loss Compensation Based on Polymeric Active-Integrated Waveguides

MEILING ZHANG[1], GUIJUN HU[1], AND XIBIN WANG[2]
[1]Department of Communication Engineering, Jilin University, Changchun 130012, China
[2]State Key Laboratory of Integrated Optoelectronics, College of Electronic Science and Engineering, Jilin University, Changchun 130012, China

Corresponding author: Xibin Wang (xibinwang@jlu.edu.cn)

This work was supported in part by the National Key Research and Development Program of China under Grant 2019YFB2203002, in part by the National Natural Science Foundation of China (NSFC) under Grant 61905088 and Grant 61875069, and in part by the Fundamental Research Funds for the Central Universities under Grant 2019JCXK-59.

ABSTRACT In this paper, an on-chip electro-optic (EO) modulator with loss compensation based on polymeric active-integrated waveguides was demonstrated. An erbium-doped waveguide amplifier was investigated and integrated with the EO modulator to compensate for signal loss. Polymeric active-integrated waveguides were based on the Mach-Zehnder interferometer structure, which consists of an amplified waveguide formed by two symmetric Y-junction branches and an EO waveguide formed by two decoupled waveguide arms. The dimensions of the polymeric active-integrated waveguides and the modulator were carefully designed and simulated. Moreover, a six-level spectroscopic model pumped at 980 nm was presented. The rate equations and propagation equations were solved, and the gain characteristics were simulated. The internal gain of 4.65 dB was achieved when the signal power was 0.1 mW at 1550 nm, the pump power was 100 mW at 980 nm, the Er^{3+} concentration was $9.3 \times 10^{25}/m^3$, and the Yb^{3+} concentration was $8.6 \times 10^{26}/m^3$ in one Y-junction branch with a length of 1.5 cm. With the integrated waveguide amplifier, the loss of the EO modulator can be compensated at 9.3 dB in the two symmetric Y-junction branches. The light output intensity was also statistically presented. The proposed device with active-integrated waveguides could be used in polymer-based photonics integrated circuits.

INDEX TERMS Integrated optics, electro-optic modulator, waveguide amplifier, polymer waveguides.

I. INTRODUCTION

Integrated optical waveguide devices are gradually becoming key components in optical telecommunication network systems [1]–[3]. The development of high- performance devices such as optical amplifiers, optical switches, optical modulators, and optical delay lines has benefited optical telecommunication systems tremendously [4]–[8]. In addition, the optical switches, and optical modulators play an indispensable role in wavelength division multiplexing (WDM) technology which serves as an important component of optical add-drop multiplexer (OADM) and optical cross-connection (OXC) applications [9], [10]. Mach-Zehnder interferometer (MZI)-type electro-optic (EO) modulators have been widely implemented in optical fiber communication systems and optical signal-processing systems [11]–[13]. An increasing number of studies have been devoted to improving the performance of MZI EO devices, such as transmission loss, driving voltage, and response speed. Combining EO materials with waveguide structures, remarkable new materials and existing structures have enhanced the performance of EO devices [14]–[16].

Nonlinear optical (NLO) polymers for EO modulators have attracted increasing attention due to their superior properties such as high EO coefficient, ultrafast frequency response, low dielectric constant, and low processing cost [17]. In recent years, many kinds of organic chromophores and NLO polymers have been investigated to fabricate EO waveguide devices [18]. EO modulators based on NLO polymers have achieved many results and shown much promise [19], [20]. However, high insertion loss still limits the performance of EO devices, especially when integrating them into photonics

The associate editor coordinating the review of this manuscript and approving it for publication was Navanietha Krishnaraj Rathinam.

integrated circuits. High insertion losses mainly occur from the coupling loss between the optical fiber and the waveguide, the scattering losses caused by fabrication, and the absorption loss from chromophores, which affect the performance of the EO modulator and impede the development of the devices. EO modulators with low insertion loss are urgently required [21], [22]. Several techniques, such as waveguide tapering, sol-gel to polymer waveguide transitions, and single-mode to multimode waveguide transitions, have been developed to solve this problem [21], [23], [24]. The passive-to-active integrated waveguide has been proposed to reduce the large absorption loss induced by the chromophores in the EO devices [25]. While the performance loss remains undesirable, designing and fabricating high-performance EO modulators with low insertion losses remains a challenge. Erbium-doped waveguide amplifiers (EDWAs) are vital components for solving this problem because the infrared emission wavelength of the Er^{3+} ion corresponds to the low-loss telecommunication window in the wavelength range of approximately 1550 nm in optical communications [26]–[28].

In this paper, an on-chip electro-optic modulator with loss compensation was demonstrated. Combined with the excellent properties of polymer such as simple processing, flexible design of optical properties and compactness, EDWA was investigated and integrated with an EO modulator to compensate for signal loss. The multi-functional device with novel structure was presented based on polymeric active-integrated waveguides. A new method for solving the bottleneck problem that high insertion loss limits the performance of the EO devices was provided, especially for integrating them into photonics integrated circuits. Polymeric active-integrated waveguides were based on an MZI structure that consisted of an amplified waveguide formed by two symmetric Y-junction branches and an EO waveguide formed by two decoupled waveguide arms. The waveguide is based on SU-8 material, which has been widely used in electro-optic modulator and optical waveguide amplifier [25], [29], [30]. Here SU-8 doped with $NaYF_4$:Er^{3+}, Yb^{3+} nanoparticles was chosen as the gain medium, because the nanoparticles with diminutive size show the advantages of adjustable luminescence, narrow bandwidth of the emission spectrum, low phonon energy, resistance to photobleaching, long fluorescent lifetime and low noise compared with the traditional dye material [31], [32]. SU-8 doped with chromophore DR19 was selected as the EO material. The dimensions of the polymeric active-integrated waveguides and the modulator were carefully designed and simulated. A formulized iteration method was presented for solving the rate equations, and the propagation equations of the Er^{3+}-Yb^{3+} codoped waveguide amplifier (EYCDWA) and the gain were numerically simulated. The internal gain of 4.65 dB was achieved when the input signal power was 0.1 mW at 1550 nm for a waveguide length of 1.5 cm, the pump power was 100 mW, the Er^{3+} concentration was $9.3 \times 10^{25}/m^3$ and the Yb^{3+}concentration was $8.6 \times 10^{26}/m^3$. The insertion loss of the EO modulator was compensated at 9.3 dB in two symmetric Y-junction branches pumped at 980 nm. The light output intensity was also numerically simulated.

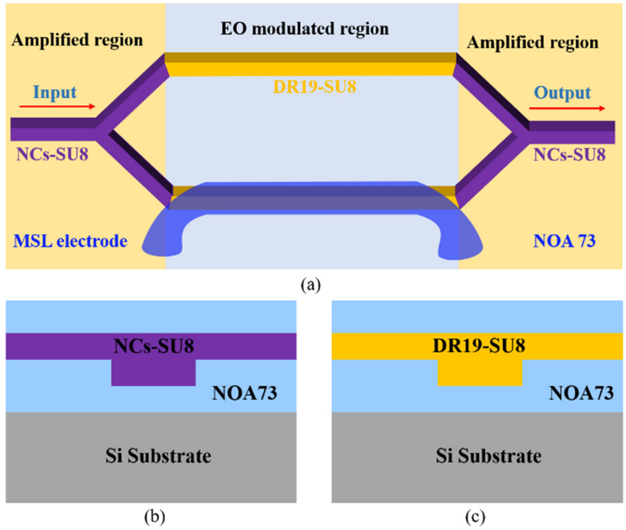

FIGURE 1. (a) Schematic diagram of a 1 × 1 polymeric EO modulator with loss compensation. (b) Cross-section of the active-integrated waveguide structure for the signal amplification region. (c) Cross-section of the active-integrated waveguide structure for the EO modulation region.

II. DEVICE DESIGN AND SIMULATION

The EO modulator with loss compensation was designed based on the polymeric active-integrated waveguides. Fig. 1(a) shows the schematic diagram of the device based on MZI that is composed of the amplified waveguide formed by two symmetric Y-junction branches and the EO waveguide formed by two decoupled waveguide arms. The length of the interference arm was 2 cm. The distance between the two interference arms was 100 μm, and the angle of the Y-junction was 0.8°. A microstrip line (MSL) electrode was introduced to form the modulating electrode. The modulating voltage is supplied to the MSL electrode, and the optical path length is changed due to the change in refractive index of the polymer waveguide caused by the EO effect. The relative phase shift of the modulation arm will excite the phase interference. Given the phase shift induced by the external electrical field, the modulated signals can be achieved in the output combiner. The signal light at 1550 nm and the pump light at 980 nm are simultaneously injected into the input waveguide. The pump light interacts with the amplified material in Y-junction branches; therefore, the signal light can be amplified, and the insertion loss will be compensated. As a consequence, the performance of the EO modulator based on the active-integrated waveguides can be significantly enhanced. Figs. 1(b) and (c) show cross-sectional views of the amplified waveguide and EO waveguide, respectively. Norland Optical Adhesive 73 (NOA73) was used as the cladding material. The commercially available material SU-8 2005 (commercially from Microchem Corp.) was used as the host material of the core layer. α-$NaYF_4$: Er^{3+},

Yb^{3+} nanoparticles (NPs) was synthesized by using a mild hydrothermal method [31]. The size of NPs has a significant effect on the waveguide amplifiers. NPs with uniform and small size can be uniformly dispersed in the polymer, which can increase the doping concentration of NPs in the polymer, but the small size NPs have a large specific surface area. A large number of surface defects and surfactant molecules can easily lead to the loss of radiative transitions in the fluorescence center and fluorescence quenching. On the other hand, though the luminescence performance of the NPs with large size can be improved, the large size NPs will cause the light scattering in the device. The NPs with the average size of 13 nm was used as the guest of the material for light amplification, which can be uniformly dispersed in the polymer with high concentration of dopant and strong fluorescence emission intensity [31]. $NaYF_4$ NPs were doped in SU-8 by a physical doping method. The Y-junction amplifiers based on $NaYF_4$/ SU-8 pumped at 980 nm can amplify the signal light and compensate for the insertion loss. The chromophore DR19 (commercially available from TCI Corp.) was used as the guest material of the EO polymer, which can be fully dissolved in SU-8 by a physical doping process. The refractive indices of the core and cladding were measured by using an ellipsometry method (J. A. Woollam., Co.M2000). The measured values of the DR19/SU-8 were 1.5846 and 1.5914 at 1550 nm and 980 nm, respectively. The measured values of the $NaYF_4$/ SU-8 were 1.5763 and 1.5822 at 1550 nm and 980 nm, respectively. The refractive indices of NOA 73 were 1.553 and 1.5611 at 1550 nm and 980 nm, respectively.

The dimensions of the polymer waveguide were carefully designed to realize the single-mode propagation. The mode field simulations at the pump and signal wavelengths were performed under the guidance of the finite difference method (FDM). The dependencies of the effective refractive indices N_{eff} of the invert-rib waveguide on the core thickness b were simulated based on the eigenvalue equations shown in Fig. 2, where the waveguide width $a = b$ and the rib height $h = 0.5b$. Fig. 2(a) shows the N_{eff} of the $NaYF_4$/ SU-8 waveguide, and Fig. 2(b) shows the N_{eff} of the DR19/SU-8 waveguide. It can be seen that both the $NaYF_4$/ SU-8 waveguide and the DR19/SU-8 waveguide can realize single-mode propagation with $b = 3$ μm ($a = 3$ μm and $h = 1.5$ μm). Moreover, the difference in the N_{eff} between the two waveguides with the same size is very small and nearly identical.

The optical field distributions of the polymeric active-integrated waveguides with this size were simulated by using the beam propagation method (BPM). Figs. 3(a) and (b) show the optical field distribution of the amplified waveguide and the EO waveguide section at 1550 nm, respectively. The optical fields are well confined in the core layer, and the mode-field diameter in the amplified section is larger than that in the modulated region, which is beneficial for decreasing the coupling loss between the optical fiber and the waveguide. The 3D optical mode field transmission of a

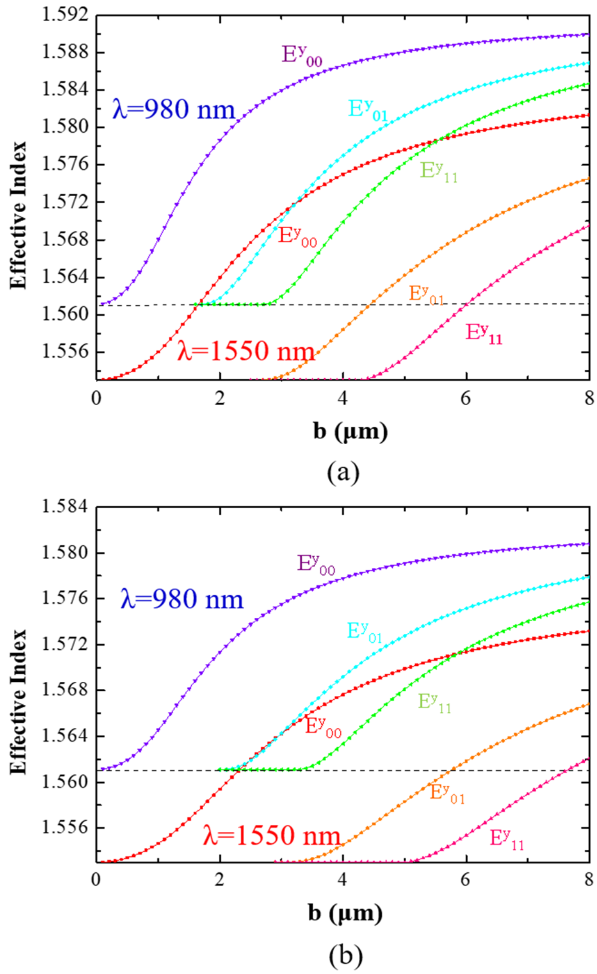

FIGURE 2. The dependencies of effective refractive N_{eff} indices on the core thickness b with a= b and h=0.5b for (a) the DR19/SU-8 waveguide and (b) the $NaYF_4$/ SU-8 waveguide.

straight waveguide was simulated trough the BPM to examine the optical transmission from the amplified waveguide to the EO waveguide. The length of the RI taper was 650 μm. Apparently, the optical signal is well transmitted from the amplified section to the modulated section with no distortion in the interconnection. The introduced RI tapers make this contribution, which can be created on the basis of a discrete step mask-shifting scheme.

Both the signal light and pump light can transmit throughout the device, which is the key to realize loss compensation. The optical field transmission for the device with an active-integrated waveguide structure was simulated by using Rsoft Beam PROP (Synopsys, Inc.). Figs. 4(a) and (b) show the light field transmission simulation results of the device at 1550 nm and 980 nm, respectively. The pump and signal light transmit well throughout the device. The input Y-junction branch served as the 3-dB power splitter at 1550 nm and 980 nm, and the symmetric Y-junction coupler acted as the output combiner.

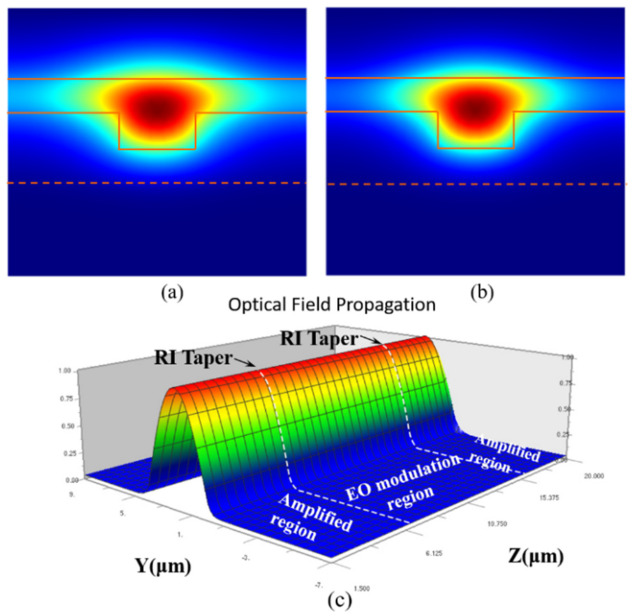

FIGURE 3. The optical field distribution of the invert-rib waveguide at 1550 nm for (a) the amplified region and (b) the modulated region. (c) The optical modal profile transmission in the active-integrated waveguide.

III. GAIN CHARACTERISTICS

It is of great importance to optimize the parameters of the waveguide combined with the gain characteristics. $NaYF_4$: Er^{3+}, Yb^{3+} NPs synthesized by the mild hydrothermal method were doped in SU-8 by the physical doping method with 0.65 wt%. The Er^{3+}-Yb^{3+} codoped six-level system was taken into consideration to obtain a more precise simulation, as shown in Fig. 5. The cooperative upconversion *(Cup)* between Er^{3+} ions and the cross-relaxed coefficient *(Ktr)* between erbium-ytterbium ions were involved. The operational principle of the amplifier pumped at 980 nm is as follows: the Yb^{3+} ions in the ground state absorb the pump energy and transition from the $^2F_{7/2}$ level to the excitation level $^2F_{5/2}$, followed by the transfer wenergy to the nearby ground state Er^{3+} ions $^4I_{15/2}$. Next, these ions are excited to the excitation level $^4I_{11/2}$. Owing to thermal relaxation, Er^{3+} ions rapidly decay to the lower metastable level $^4I_{13/2}$ and remain there longer. When the pump power exceeds the threshold power, population inversion occurs between $^4I_{15/2}$ and $^4I_{13/2}$. Then, the Er^{3+} ions in the $^4I_{13/2}$ level transition down to the ground level $^4I_{15/2}$ and emit the photons with the same frequency as that of the signal realizing the amplification function for the signal. Here, the amplified spontaneous emission (*ASE*) was neglected [26], [27].

Therefore, the simplified versions of the rate equations are obtained using the overlap integral method, where N_1, N_2, N_3 and N_4 are defined as the concentrations of Er^{3+} in the $^4I_{15/2}$, $^4I_{13/2}$, $^4I_{11/2}$ and $^4I_{9/2}$ energy states, and N_5 and N_6 are defined as the concentrations of Yb^{3+} in the $^2F_{5/2}$ and $^2F_{7/2}$ energy states, respectively. N_{Er} is the total Er^{3+} ion concentration and N_{Yb} is the total Yb^{3+} ion concentration.

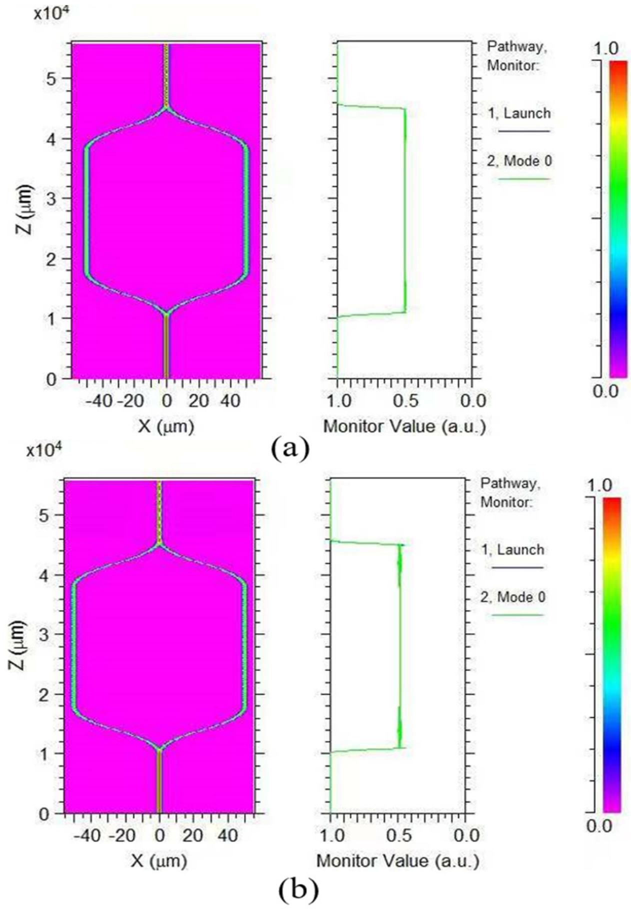

FIGURE 4. Single-mode optical field transmission of the EO device simulated by Rsoft: (a) at a wavelength of 1550 nm; (b) at a wavelength of 980 nm.

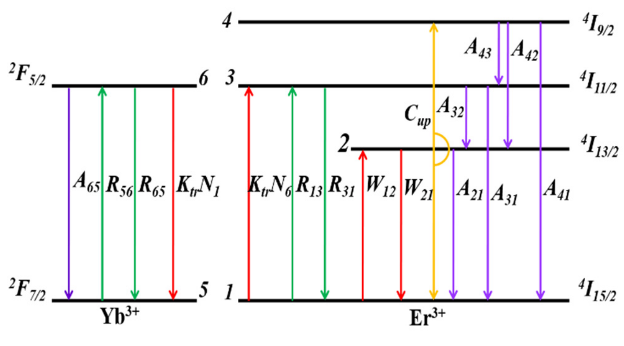

FIGURE 5. Energy level transitions for Er^{3+}–Yb^{3+} codoped six-level system (980 nm pump).

Under steady-state conditions, the population densities maintain the dynamic balances considered in this system. The set of rate equations under the boundary conditions were formulated and solved. Incorporating the signal and pump propagation equations, the gain characteristics were investigated using the Runge-Kutta method under uniform doping conditions. The gain G was defined as follows [33]:

$$G\,(dB) = 10lg\frac{P_S(z)}{P_S(0)} \tag{1}$$

TABLE 1. Parameter values of $NaYF_4$: Er^{3+}, Yb^{3+} NPs-doped SU-8 material.

Symbol	Full name	Quantity
σ_{12}	Absorption cross-section of Er^{3+} at 1550 nm	9.47×10^{-25} m^2
σ_{21}	Emission cross-section of Er^{3+} at 1550 nm	1.65×10^{-25} m^2
σ_{13}	Absorption cross-section of Er^{3+} at 980 nm	2.32×10^{-25} m^2
σ_{56}	Absorption cross-section of Yb^{3+} at 980 nm	1×10^{-24} m^2
σ_{65}	Emission cross-section of Yb^{3+} at 980 nm	1×10^{-24} m^2
τ_{21}	Er^{3+} emission lifetime of $^4I_{13/2}$	2.02 ms
τ_{32}	Er^{3+} nonradiative lifetime of $^4I_{11/2}$	38.49 ms
τ_{65}	Yb^{3+} emission lifetime of $^2F_{7/2}$	1.3 ms
A	Cross-section of the active region	24.85 μm^2
C_{up}	Up-conversion coefficient	8.42×10^{-23}m^{2}s^{-1}
K_{tr}	Cross-relaxation coefficient	4.4×10^{-22}m^{2}s^{-1}
N_{Er}	Erbium ion density	9.3×10^{25} /m^3
N_{Yb}	Ytterbium ion density	8.6×10^{26} /m^3
Γs	Overlapping factor of the signal laser	0.74
Γp	Overlapping factor of the pump laser	0.88

It is difficult to test all parameters of the gain medium implemented in the simulation accurately. Incorporating the Judd-Ofelt theory, the absorption and emission spectra are characterized, and the parameter values of $NaYF_4$/ SU-8 are calculated as shown in Table 1. The transmission loss of the waveguide amplifier measured by the cutback method is approximately 1.5 dB/cm, and the gain curves were simulated. Fig. 6(a) shows the gain as a function of pump power at 980 nm for different overlapping factors. The overlap integral factor plays a decisive role in the gain. The formula is defined as follows [34]:

$$\Gamma_{S,P} = \iint \Psi(x, y)\, dxdy = \iint_A \Psi(x, y)\, dxdy \tag{2}$$

where Γ_P and Γ_S are the overlap factors of the pump and the signal, respectively. A is the area of the cross-section of the waveguide core.

The internal gain increases gradually with increasing pump power. When the pump power exceeds the threshold power, the gain demonstrates its tendency to be saturated. As the overlapping factors increase, the gain value increases, as does the threshold power. The overlapping factors of the $NaYF_4$/ SU-8 embedded waveguide are 0.74 at 1550 nm and 0.88 at 980 nm, the threshold of which is 100 mW. From the formula above, the overlap factors are altered according to the various waveguide cross-section dimensions. As illustrated in the simulation results, the overlapping factors relevant to the dimensions of the waveguide exceedingly impact the gain. It is of great necessity to have the dimension designed accurately and legitimately. As stated above, a pump power of 100 mW is chosen. Then, the waveguide length is optimized in accordance. Fig. 6(b) indicates the internal gain as a function of waveguide length for different pump powers. As the waveguide length increases, the gain increases gradually to a maximum and then decreases continually. The waveguide length corresponding to the maximum gain is called the optimal waveguide length. When the pump power increases, the gain corresponding to the optimal length performs in the same way, which is the result of the pump power constantly consumed in the transmission along the waveguide. After reaching the optimal waveguide length, the pump power is smaller than the threshold power, and the amplification shuts off, with transmission loss causing negative gain when the length is too long. Upon increasing the input pump power, the pump power will reach the threshold power in the farther transmission direction. During this period, the device keeps amplifying the signal light so that the maximum gain is improved. Therefore, the optimal waveguide length of 1.5 cm is chosen with the pump power of 100 mW.

The concentration of Er^{3+} is a significant parameter that directly impacts the gain. Thus, for a pump power of 100 mW, the internal gain versus coordinate Er^{3+} concentration of the $NaYF_4$/ SU-8 for different signal powers is shown in Fig. 6(c). The gain increases with decreasing signal power. When the signal power is 0.01 mW, the gain curve almost overlaps with the gain curve that the input signal power is 0.1 mW, and the increase in the gain tends to be saturated. A small signal power is desirable, which shows the dependence given by (1). Fig. 6(c) indicates that as the Er^{3+} concentration increases, the gain increases to the maximum value with the optimal Er^{3+} concentration and then decreases. Theoretically, when the pump power is sufficient, the higher the Er^{3+} concentration is, the greater the gain achieved and the higher the threshold power required. This is because the threshold pumping power represents the minimum pump power for the occurrence of the population inversion between the metastable energy level and the ground state energy level. For a constant pump power, Er^{3+} can be fully motivated with the optimal concentration, and the maximum gain is achieved. As the Er^{3+} concentration continues to increase, more pump power is desired, the existing pump power can't meet the demand of the threshold power, population inversion is not adequate, and the gain declines gradually. Excessive Er^{3+} ion doping can lead to concentration quenching caused by agglomeration in the experiment [29], [31]. Consequently, the Er^{3+} concentration can't be excessively high. The optimal concentration is 9.3×10^{25}/m^3 on behalf of achieving a high gain. Ytterbium ions staggered around erbium ions codoped as a sensitizer can increase the effective concentration of Er^{3+} and effectively prevent quenching. The Yb^{3+} concentration has a substantial impact on the gain, and then the Yb^{3+} concentration is optimized. The internal gain curves as a function of Yb^{3+} concentration for different Er^{3+} concentrations are shown in Fig. 6(d). From Fig. 6(d), as the Yb^{3+} concentration increases, the gain increases to a maximum and then decreases, the reason for which is similar to Er^{3+}. As the Er^{3+} concentration increases, the optimal concentration decreases. The optimal Yb^{3+} concentration is 8.6×10^{26}/m^3, when the pump power is 100 mW, the signal power is 0.1 mW, and

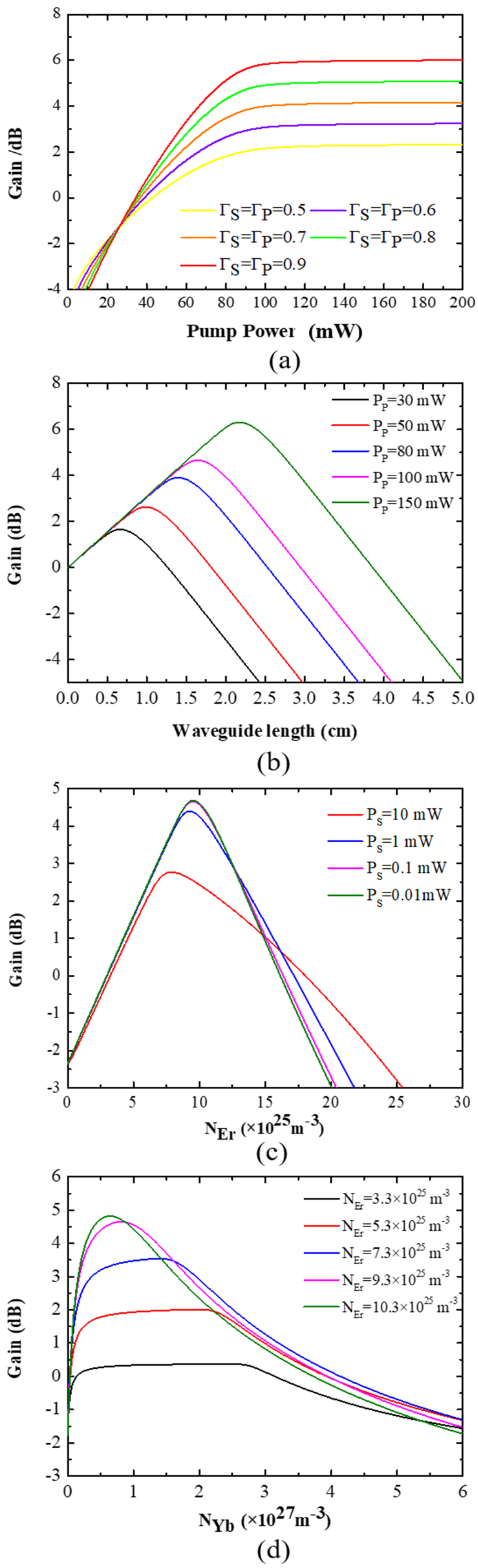

FIGURE 6. **(a) Gain versus coordinate pump power at 980 nm for different overlapping factors. (b) Gain versus coordinate waveguide length for different pump power. (c) Gain as a function of Er^{3+} concentration for different signal power. (d) Gain as a function of Yb^{3+} concentration for different Er^{3+} concentration.**

the Er^{3+} concentration is $9.3 \times 10^{25}/m^3$. A maximum gain of 4.65 dB is demonstrated with an optimal waveguide length of 1.5 cm. Thus, a relative gain of 9.3 dB in two symmetric Y-junction branches can be achieved.

IV. ANALYSIS OF EO MODULATION PERFORMANCE

With the integrated waveguide amplifier, the loss of the EO modulator can be compensated. For the EO waveguide, the core layer is formed with a guest-host EO material DR19/SU-8 synthesized by the means of a simple physical doping process. The chromophore DR19, as the guest material, was incorporated with the SU-8 material at 4.5% by weight. The SU-8 network is heavily cross-linked through thermal UV-curing, and then the guest chromophore DR19 is compromised, which provides high stability. Moreover, the selected host material SU-8 2005 is the same as the host material of the amplified material, which helps to avoid phase separation in the interconnection of the active-integrated waveguide. The EO coefficient r of DR19/SU-8 was approximately 19.6 pm V^{-1}.

The performance of the EO modulator is closely related to the insertion loss of the device. The proposed polymeric active-integrated waveguide with loss compensation ameliorating the loss characteristics will affect the signal output intensity and thus impact the EO modulation performance of the device, which must be analyzed. The output field intensity I_{out} of the MZI-type EO modulator depends on the phase difference of the beams in the two MZI arms. The I_{out} can be defined as:

$$\boldsymbol{I_{out}} = \boldsymbol{I_0}(1 + \boldsymbol{cos}(\boldsymbol{\varphi_0} + \boldsymbol{\Delta\varphi})) \tag{3}$$

where I_0 is the light intensity in each arm of the MZI and φ_0 is the phase deviation arising from the optical path difference between the two MZI arms. $\Delta\varphi$ is the phase difference due to the EO effect, which can be approximated by:

$$\boldsymbol{\Delta\varphi} = -\frac{\boldsymbol{k \cdot r \cdot V \cdot L \cdot \Gamma \cdot n^3}}{\boldsymbol{2\omega}} \tag{4}$$

where k is the wavenumber, r is the EO coefficient, V is the applied modulating voltage, w is the electrode distance, L is the interaction length, and Γ is the overlap integral between the applied electric field and the optical mode. The interelectrode distance is 7.5 μm. The overlap integral between the applied electric field and the optical mode is approximately 0.75.

Based on the above theoretical basis, a sinusoidal signal with 100 kHz is applied to the electrode, and the peak-to-peak value V_{p-p} is 5 V. The normalized output light intensity I_{out} of the active-integrated waveguide with and without loss compensation is analyzed, as shown in Fig. 7. When the core of the EO modulator is completely formed with the EO polymer (i.e., the EO modulator without loss compensation), $I_{out,1}$ is calculated in Fig. 7 and shown as the black curve. When the input Y-junction, as the amplified waveguide, is integrated with the EO modulator, the normalized output light intensity

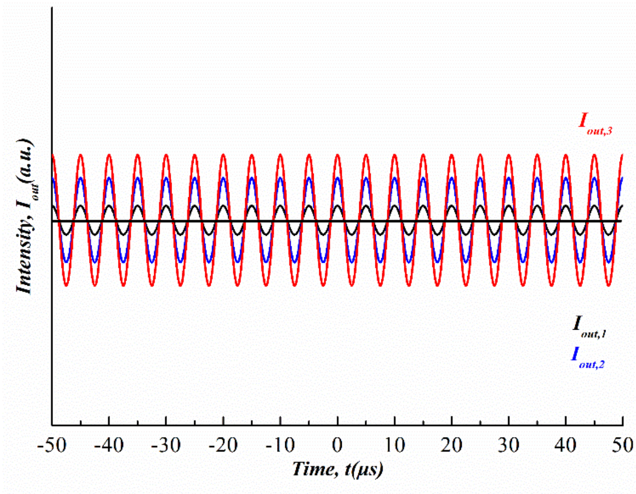

FIGURE 7. The normalized output light intensity of the device with and without loss compensation.

$I_{out,2}$ is simulated, as shown in Fig. 7, as the blue curve. It can be seen that with the integrated amplified waveguide, the output response amplitude is increased. An optical gain of 4.65 dB can be obtained. Furthermore, when input and output Y-junctions, as the amplified waveguides, are both integrated with the EO modulator, the normalized output light intensity $I_{\mathrm{out},3}$ is simulated, as shown in Fig. 7, as the red curve. The entire compensation process can be explained as follows. First, the input optical signal is compensated through the input Y-junction amplified waveguide. After modulating by the applied modulating voltage, the signal light continues to transmit along the waveguide, and the output signal proceeds with amplification as crossing over the output Y-junction amplified waveguide. The output light intensity is enhanced compared with $I_{out,2}$. Obviously, the output light intensity and the response amplitude of the EO modulator with the active-integrated waveguide are dramatically promoted due to the loss compensation on the basis of the simulated results. This is beneficial for improving the performance of the EO device. Moreover, the performance of the device can be further improved by introducing some gain materials with better performance and EO materials with larger EO coefficients [26], [32], [35], [36].

V. CONCLUSIONS

In summary, an on-chip electro-optic modulator with loss compensation based on polymeric active-integrated waveguides is demonstrated. An integrated waveguide composed of an amplified waveguide formed by two symmetric Y-junction branches and an EO waveguide made of two decoupled waveguide arms is presented. The erbium-doped waveguide amplifier is integrated with the EO modulator to compensate for signal loss. The dimensions of the active-integrated waveguide are designed. The gain and EO modulation characteristics are numerically simulated. The simulation results show that the output light intensity and the response amplitude of the EO modulator with the active-integrated waveguide are dramatically promoted due to loss compensation. This is beneficial for improving the performance of the EO device. The proposed polymeric active-integrated waveguide structure with the simple processing is a good candidate for integrated optical waveguide devices in optical telecommunication network systems.

REFERENCES

[1] S. Dutta, E. A. Goldschmidt, S. Barik, U. Saha, and E. Waks, "Integrated photonic platform for rare-earth ions in thin film lithium niobite," *Nano Lett.*, vol. 20, no. 1, pp. 741–747, Nov. 14, 2019.

[2] M. J. R. Heck, J. F. Bauters, M. L. Davenport, D. T. Spencer, and J. E. Bowers, "Ultra-low loss waveguide platform and its integration with silicon photonics," *Laser Photon. Rev.*, vol. 8, no. 5, pp. 667–686, Mar. 2014.

[3] K.-I. Sato, "Realization and application of large-scale fast optical circuit switch for data center networking," *J. Lightw. Technol.*, vol. 36, no. 7, pp. 1411–1419, Apr. 1, 2018.

[4] H. Lee, T. Chen, J. Li, O. Painter, and K. J. Vahala, "Ultra-low-loss optical delay line on a silicon chip," *Nature Commun.*, vol. 3, no. 1, p. 867, May 2012.

[5] Q. Xu, M. H. Jiang, D. H. Niu, X. B. Wang, L. L. Wang, K. S. Chiang, and D. M. Zhang, "Fast and low-power thermo-optic switch based on organic-inorganic hybrid strip-loaded waveguides," *Opt. Lett.*, vol. 43, no. 20, pp. 5102–5105, Oct. 2018.

[6] J. Rönn, W. Zhang, A. Autere, X. Leroux, L. Pakarinen, C. Alonso-Ramos, A. Säynätjoki, H. Lipsanen, L. Vivien, E. Cassan, and Z. Sun, "Ultra-high on-chip optical gain in erbium-based hybrid slot waveguides," *Nature Commun.*, vol. 10, no. 1, p. 432, Jan. 2019.

[7] Y. Cao, D. Zhang, Y. Yang, B. Lin, J. Lv, X. Yang, H. Zhao, F. Wang, B. Li, and Y. Yi, "Dispersed-monolayer graphene-doped polymer/silica hybrid mach-zehnder interferometer (MZI) thermal optical switch with low-power consumption and fast response," *Polymers*, vol. 11, no. 11, p. 1898, Nov. 2019.

[8] X. Y. Wang, L. J. Zhou, R. F. Li, J. Y. Xie, L. J. Lu, K. Wu, and J. P. Chen, "Continuously tunable ultra-thin silicon waveguide optical delay line," *Optica*, vol. 4, no. 5, pp. 507–515, May 20, 2017.

[9] I. A. Pshenichnyuk, G. I. Nazarikov, S. S. Kosolobov, A. I. Maimistov, and V. P. Drachev, "Edge-plasmon assisted electro-optical modulator," *Phys. Rev. B, Condens. Matter*, vol. 100, no. 19, Nov. 2019, Art. no. 195434.

[10] H. Lu, X. Liu, L. Wang, Y. Gong, and D. Mao, "Ultrafast all-optical switching in nanoplasmonic waveguide with Kerr nonlinear resonator," *Opt. Express*, vol. 19, no. 4, pp. 2910–2915, Feb. 2011.

[11] M.-H. Jiang, X.-B. Wang, Q. Xu, M. Li, D.-H. Niu, X.-Q. Sun, F. Wang, Z.-Y. Li, and D.-M. Zhang, "High-speed electro-optic switch based on nonlinear polymer-clad waveguide incorporated with quasi-in-plane coplanar waveguide electrodes," *Opt. Mater.*, vol. 75, pp. 26–30, Jan. 2018.

[12] S. Kumar and S. K. Raghuwanshi, "High speed optical 4-bit twisted ring counter using electro-optic effect of mach-zehnder interferometer," *Opt. Quantum Electron.*, vol. 48, no. 1, p. 42, Jan. 2016.

[13] A. M. Gutierrez, A. Brimont, J. Herrera, M. Aamer, D. J. Thomson, F. Y. Gardes, G. T. Reed, J.-M. Fedeli, and P. Sanchis, "Analytical model for calculating the nonlinear distortion in silicon-based electro-optic mach–zehnder modulators," *J. Lightw. Technol.*, vol. 31, no. 23, pp. 3603–3613, Dec. 2013.

[14] D. Sun, Z. Hu, S. Abdul-Majid, R. Vandusen, Q. Zheng, I. Hasan, N. G. Tarr, S. Bidnyk, and T. J. Hall, "Limitation factor analysis for silicon-on-insulator waveguide Mach-Zehnder interference-based electro-optic switch," *J. Lightw. Technol.*, vol. 29, no. 17, pp. 2592–2600, Sep. 2011.

[15] A. Rao, A. Patil, P. Rabiei, A. Honardoost, R. DeSalvo, A. Paolella, and S. Fathpour, "High-performance and linear thin-film lithium niobate Mach-Zehnder modulators on silicon up to 50 GHz," *Opt. Lett.*, vol. 41, no. 24, pp. 5700–5703, Dec. 2016.

[16] M. B. He, M. Y. Xu, Y. X. Ren, J. Jian, Z. L. Ruan, Y. S. Xu, S. Q. Gao, S. H. Sun, X. Q. Wen, L. D. Zhou, L. Liu, C. J. Guo, H. Chen, S. Y. Yu, L. Liu, and X. Cai, "High-performance hybrid silicon and lithium niobate Mach-Zehnder modulators for 100 Gbit s(-1) and beyond," *Nature Photon.*, vol. 13, no. 5, p. 359, May 2019.

[17] H. Ma, A. K.-Y. Jen, and L. R. Dalton, "Polymer-based optical waveguides: Materials, processing, and devices," *Adv. Mater.*, vol. 14, no. 19, pp. 1339–1365, Oct. 2002.

[18] X. Wang, J. Sun, L. Jin, J. Meng, Y. Yan, C. Chen, F. Wang, and D. Zhang, "Fabrication of SU-8-based electro-optic switch using all-wet etching technique," *Modern Phys. Lett. B*, vol. 27, no. 4, Feb. 2013, Art. no. 1350024.

[19] J. Liu, G. Xu, F. Liu, I. Kityk, X. Liu, and Z. Zhen, "Recent advances in polymer electro-optic modulators," *RSC Adv.*, vol. 5, no. 21, pp. 15784–15794, 2015.

[20] S. W. Wang, W. L. Su, Y. H. Li, R. W. Zhang, X. B. Wang, and D. M. Zhang, "Effect of solvent vapor annealing on polymer thin films and the application on nonlinear optical fields," *J. Mater. Chem. C*, vol. 2, no. 41, pp. 8662–8666, Jun. 2014.

[21] C. T. DeRose, D. Mathine, Y. Enami, R. A. Norwood, J. Luo, A. K.-Y. Jen, and N. Peyghambarian, "Electrooptic polymer modulator with single-mode to multimode waveguide transitions," *IEEE Photon. Technol. Lett.*, vol. 20, no. 12, pp. 1051–1053, Jun. 2008.

[22] Y. Enami, G. Meredith, N. Peyghambarian, M. Kawazu, and A. K.-Y. Jen, "Hybrid electro-optic polymer and selectively buried sol-gel waveguides," *Appl. Phys. Lett.*, vol. 82, no. 4, pp. 490–492, Jan. 2003.

[23] T. Matsui, K. Komatsu, O. Sugihara, and T. Kaino, "Simple process for fabricating a monolithic polymer optical waveguide," in *Opt. Lett.*, vol. 30, no. 9, pp. 970–972, May 1, 2005.

[24] S. W. Ahn, W. H. Steier, Y. H. Kuo, M. C. Oh, and H. J. Lee, "Integration of electro-optic polymer modulators with low-loss fluorinated polymer waveguides," *Opt. Lett.*, vol. 27, no. 23, pp. 2109–2111, Dec. 2002.

[25] X. B. Wang, M. H. Jiang, S. Q. Sun, J. W. Sun, Y. J. Yi, C. M. Chen, X. Q. Sun, F. Wang, Z. C. Cui, and D. M. Zhang, "Demonstration of a high-speed electro-optic switch with passive-to-active integrated waveguide based on SU-8 material," *RSC Adv.*, vol. 6, no. 55, pp. 50166–50172, 2016.

[26] M. Zhang, W. Zhang, F. Wang, D. Zhao, C. Qu, X. Wang, Y. Yi, E. Cassan, and D. Zhang, "High-gain polymer optical waveguide amplifiers based on core-shell $NaYF_4/NaLuF_4$: Yb^{3+}, Er^{3+} NPs-PMMA covalent-linking nanocomposites," *Sci. Rep.*, vol. 6, no. 1, p. 36729, Nov. 2016.

[27] Y. Cao, B. Lin, Y. Sun, Y. Yi, Y. Liu, J. Zheng, F. Wang, and D. Zhang, "Polymer-silica hybrid on-chip amplifier with vertical pumping method," *Sci. Rep.*, vol. 8, no. 1, p. 13682, Sep. 2018.

[28] D. Brüske, S. Suntsov, C. E. RÜTER, and K. Detlef, "Efficient ridge waveguide amplifiers and lasers in Er-doped lithium niobate by optical grade dicing and three-side Er and Ti in-diffusion," *Opt. Express*, vol. 25, no. 23, pp. 29374–29379, Nov. 2017.

[29] P. C. Zhao, M. L. Zhang, T. J. Wang, X. Y. Liu, X. S. Zhai, G. S. Qin, W. P. Qin, and D. M. Zhang, "Optical amplification at 1525nm in $BaYF_5$: 20% Yb^{3+}, 2% Er^{3+} nanocrystals doped SU-8 polymer Waveguide," *J. Nanomater.*, vol. 2014, Jun. 2014, Art. no. 153028.

[30] E. Nitiss, A. Tokmakovs, K. Pudzs, J. Busenbergs, and M. Rutkis, "All-organic electro-optic waveguide modulator comprising SU-8 and nonlinear optical polymer," *Opt. Express*, vol. 25, no. 25, pp. 31044–31306, Dec. 2017.

[31] G. C. Xing, M. L. Zhang, T. H. Sun, Y. W. Fu, Y. L. Huang, J. Shao, J. R. Liu, F. Wang, and D. M. Zhang, "Polymer waveguide thermo-optical switch with loss compensation based on $NaYF_4$: 18% Yb^{3+}, 2% Er^{3+} nanocrystals," *Chin. Phys. B.*, vol. 27, no. 55, Oct. 2018, Art. no. 114218.

[32] T. J. Wang, D. Zhao, M. L. Zhang, J. Yin, W. Y. Song, Z. X. Jia, X. B. Wang, G. S. Qin, W. P. Qin, F. Wang, and D. M. Zhang, "Optical waveguide amplifiers based on $NaYF_4$: Er^{3+}, Yb^{3+} NPs-PMMA covalent-linking nanocomposites," *Opt. Mater. Express*, vol. 5, no. 3, pp. 469–478, Mar. 2015.

[33] S. Suntsov, C. E. Rüter, and D. Kip, "Er:Ti:$LiNbO_3$ ridge waveguide optical amplifiers by optical grade dicing and three-side er and ti in-diffusion," *Appl. Phys. B*, vol. 123, no. 4, p. 118, Apr. 2017.

[34] P. C. Zhao, H. Q. Chen, C. T. Zheng, F. Wang, D. M. Zhang, and C. S. Ma, "Gain and noise characteristics of phosphate glass Er^{3+}-Yb^{3+} co-doped waveguide amplifiers," *Opt. Quantum Electron.*, vol. 46, no. 12, pp. 1571–1587, Dec. 2014.

[35] Y. Jouane, Y. C. Chang, D. Zhang, J. Luo, A. K. Y. Jen, and Y. Enami, "Unprecedented highest electro-optic coefficient of 226 pm/V for electro-optic polymer/TiO_2 multilayer slot waveguide modulators," *Opt. Express*, vol. 22, no. 22, pp. 27725–27732, Nov. 2014.

[36] M. Li, H. Zhang, Y. Zhang, B. Hou, C. Li, X. Wang, J. Zhang, L. Xiao, Z. Cui, and Y. Ao, "Facile synthesis of benzothiadiazole-based chromophores for enhanced performance of second-order nonlinear optical materials," *J. Mater. Chem. C*, vol. 4, no. 38, pp. 9094–9102, 2016.

MEILING ZHANG received the B.S. degree in electronic science and technology and the M.S. and Ph.D. degrees in microelectronics and solid electronics from Jilin University, in 2012, 2015, and 2018, respectively. She is currently a Lecturer with the Department of Communication Engineering, Jilin University. Her current research interests include polymer planar optical waveguide devices and optical beamforming.

GUIJUN HU was born in Liaoning, China, in 1970. He received the B.S. and M.S. degrees in optical engineering from the University of Northeast Normal University, in 1996, and the Ph.D. degree in microelectronics and solid state electronics from Jilin University.

From 2000 to 2005, he was a Senior Lecturer with the Department of Communication Engineering, Jilin University, where he has been a Professor, since 2006. He is the author of more than 100 articles and more than ten inventions. His research interests include optical fiber communication, optoelectronics, and fiber sensor. He is a member of the Society of Photo-Optical Instrumentation Engineers (SPIE).

XIBIN WANG received the B.S. degree in electronic science and technology, and the M.S. and Ph.D. degrees in microelectronics and solid electronics from Jilin University, Changchun, China, in 2008, 2010, and 2013, respectively. He is currently an Associate Professor with Jilin University. He is also with the State Key Laboratory of Integrated Optoelectronics. His current research interests include second-order nonlinear optical polymer materials, as well as active and passive polymeric waveguide and PLC devices for optical interconnect and sensor applications.